Philosophical Magazine

ISSN: 1478-6435 (Print) 1478-6443 (Online) Journal homepage: https://www.tandfonline.com/loi/tphm20

Annealing behaviour of ultrafine-grained aluminium

Pei-Ling Sun, Yonghao Zhao, Tien-Yu Tseng, Jiunn-Ren Su & Enrique J. Lavernia

To cite this article: Pei-Ling Sun, Yonghao Zhao, Tien-Yu Tseng, Jiunn-Ren Su & Enrique J. Lavernia (2014) Annealing behaviour of ultrafine-grained aluminium, Philosophical Magazine, 94:5, 476-491, DOI: 10.1080/14786435.2013.856526

To link to this article: https://doi.org/10.1080/14786435.2013.856526

Philosophical Magazine, 2014
Vol. 94, No. 5, 476–491, http://dx.doi.org/10.1080/14786435.2013.856526

Taylor & Francis
Taylor & Francis Group

Annealing behaviour of ultrafine-grained aluminium

Pei-Ling Sun[a]*, Yonghao Zhao[b], Tien-Yu Tseng[c], Jiunn-Ren Su[c] and Enrique J. Lavernia[d]

[a]*Department of Materials Science and Engineering, Feng Chia University, Taichung 40724, Taiwan;* [b]*Nanostructural Materials Research Center, School of Materials Science and Engineering, Nanjing University of Science and Technology, Nanjing 210094, China;* [c]*New Materials Research and Development Department, China Steel Corporation, Kaohsiung 81233, Taiwan;* [d]*Department of Chemical Engineering and Materials Science, University of California, Davis, CA 95616, USA*

(*Received 25 February 2013; accepted 10 October 2013*)

Ultrafine-grained (UFG) aluminium, processed under fast cooling rate conditions (12 K s^{-1}) following hot rolling (water quenched) exhibits enhanced thermal stability due to an increase in concentration of solid solution atoms, relative to the furnace cooled material. The influence of fraction recrystallized on yield stress and uniform elongation is reported to exhibit a slight deviation from the linear behaviour that is anticipated on the basis of the rule-of-mixtures. This result was rationalized on the basis of differences in the spatial distributions of the UFG and coarse grains and/or dislocation recovery mechanisms.

Keywords: aluminium; hot and cold rolling; annealing; cooling rate; mechanical property

1. Introduction

Ultrafine-grained (UFG) and nanostructured (NS) materials exhibit enhanced strength as compared to that of their coarse grain (CG) counterparts, which has been rationalized, in part, on the basis of a Hall-Petch strengthening mechanism. However, bulk NS materials usually have a low thermal stability [1], inferior ductility [2,3] and relatively steep manufacturing costs, which are major concerns for technological applications and consequently have evolved into mayor areas of research. The low thermal stability of bulk NS materials is attributable to the large amount of enthalpy that is stored in the large grain boundary volume associated with NS grains (i.e. 1–100 nm).

Inspection of the literature reveals that NS and UFG elemental metals with low melting temperatures, such as Sn, Pb, Al and Mg, tend to exhibit significant grain growth, even at room temperature [4]. Even in the case of pure metals with intermediate and high melting temperatures, such as pure Cu, Ag and Pd, grain growth has been reported to occur at much lower temperatures (or even at room temperature) than those observed for recrystallization (RX) of metals subjected to heavy cold deformation [5]. This is an interesting observation because Pd has a high melting point of 1552 °C and hence in this case room temperature is equivalent to a low homologous temperature

*Corresponding author. Email: plsun@fcu.edu.tw

($0.16T_m$). Even for nominally pure metals, such as Fe [6], Cu [7] and Ni [8], significant grain growth has been reported to occur at annealing temperature less than $0.5T_m$ in the case of NS and UFG samples. The poor thermal stability of NS materials limits their application to low homologous temperatures. Recently, both kinetic and thermodynamic strategies have been proposed to stabilize these nanostructures [9]. The kinetic stabilization strategy involves a reduction of grain boundary mobility, and includes mechanisms such as: second phase drag [10], solute drag [11] and chemical ordering [12]. The thermodynamic stabilization strategy involves decreasing the specific grain boundary energy by solute segregation to the grain boundary [13,14]. Successful implementation of these strategies could lead to NS grains that are stable up to temperatures equivalent to $0.8T_m$ [15]. In addition to temperature, annealing time can also affect grain growth. Chookajorn et al. [16] used thermodynamic calculations to determine the suitable binary alloys can be stabilized by grain boundary segregation during annealing. Corresponding experiments of the W-Ti alloys prepared by ball-milling confirmed significant thermal stability at prolonged annealing time.

In addition to low thermal stability, UFG/NS metals also suffer from poor tensile ductility and this behaviour has been attributed to the onset of plastic instability (necking) at the early stage of tensile deformation, in which the small grain size limits dislocation slip and dislocation–dislocation interactions. Consequently, fewer dislocation interactions limit the extent of work hardening rate in UFG/NS materials. Ductility represents an essential material attribute for many structural applications in which delaying and/or limiting catastrophic failure is a requirement. Not surprisingly, numerous studies have been published describing strategies to improve the ductility of UFG/NS materials [17]. Among these strategies, introducing a bi-modal or multi-modal grain size distribution has been shown to be broadly applicable to many material systems [2,18–21]. These bi-modal or multi-modal materials usually have a wide grain size distribution ranging from nanometer to micrometer sizes [21]. The UFG grains in bi-modal materials can promote a high strength by limiting dislocation movement, whereas the micron-sized grains occupy a larger volume fraction of the microstructure, thus increasing their effect on the behaviour of the aggregate, such as ductility, by suppressing crack growth and facilitating plastic deformation [19]. In addition to the incorporation of bi-modal or multi-modal microstructures, various other strategies have also been devised in an effort to attain a better balance of strength and ductility; these include: grain boundary engineering [3,22], modifying stacking fault energy [23,24] and incorporating nanometric second-phase particles or solid solution atoms [25,26].

In our previous study [26], we demonstrated that controlled quenching of hot rolled Al can be used as a straightforward strategy to obtain different degrees of solid solubility, and accordingly, different microstructures. For example, the water quenched (WQ) sample contained a higher concentration of atoms in solid solution and the resultant microstructure after cold rolling consisted of smaller grain size and higher proportion of high angle boundaries relative to those in the furnace cooled (FC) sample. Moreover, our results showed that the microstructure of the WQ sample led to improvements in yield stress (YS), ultimate tensile stress (UTS) and tensile elongation over those of the FC sample. Microstructural analyses revealed that the origin of the high strength of the WQ UFG Al is attributable to smaller grain dimensions in the quenched and rolled material. The measured enhanced ductility was rationalized on the basis of improved dislocation accumulation and a higher rate of strain hardening due to solid solution

pinning during plastic deformation and higher fraction of high-angle grain boundaries [26].

The present work demonstrates that the WQ sample, not only possesses superior mechanical properties, but also enhanced thermal stability, as evidenced by the observation that RX temperature increases with solute content. In this study, heat treatments were conducted on the as-cold rolled WQ and FC samples and some samples with bi-modal grain size distribution were obtained. Examination of the relationship between stress/ductility and RX grain fraction reveals slight deviations from the results anticipated on the basis of the rule-of-mixtures. This is attributed to the differences in microstructural characteristics, such as the spatial distributions of the UFG and CG grains, and or possibly different size differences between the micro-grains and the UFG matrix [27].

2. Experimental

A commercial purity aluminium, AA1050, with the chemical composition in wt.% of 0.089 Si, 0.216 Fe, 0.001 Cu, 0.02 Ti and balance Al was first homogenized at 590 °C for 9 h, followed by hot rolling from a thickness of 110 to 6 mm and then cooled with distinct cooling rates: FC and WQ. The two samples were then cold rolled to a final thickness of 0.3 mm, which corresponds to a total reduction of ~95%.

The as-cold rolled specimens were annealed at temperatures ranging from 160 to 340 °C for 1 h to study their annealing behaviour. Isothermal annealing was also conducted on the two materials from 10 to 480 min at 240 °C. Grain morphology and grain size of the as-cold rolled and annealed transverse planes were examined by the use of optical microscope. Transverse planes of the as-cold rolled FC and WQ specimens were prepared for transmission electron microscope (TEM) observation. Samples were mechanically ground to a thickness of ~150 μm and final polishing was done followed a standard twin-jet polishing method with an electrolyte of 25% nitric acid and 75% methanol at −30 °C and 15 V. Microstructures of the as-cold rolled samples were characterized in a Philips CM200 TEM at 200 kV. Grain length, grain width and grain aspect ratio were then determined based on the TEM images. The boundary structures of the FC and WQ samples were analysed by the use of TEM. By performing microdiffraction analysis, Kikuchi pattern of each grain can be recorded by a CCD camera, and indexed by a commercially available program (TOCA, TSL Inc., Utah, USA). The misorientation between adjacent grains was then calculated as 'angle/axis pair', where the minimum misorientation angle is selected from the 24 equivalent solutions calculated according to the symmetry of the FCC structure [28]. Five areas were examined to obtain boundary misorientation distributions and over 400 boundaries were analysed in both FC and WQ samples. The texture evolution during annealing was investigated by the use of orientation distribution functions (ODF), which was obtained from X-ray pole figure analysis.

Uniaxial tensile tests were conducted on the as-cold rolled and annealed samples with an initial strain rate of $1.67 \times 10^{-3}\,s^{-1}$ at ambient temperature. The gauge section had a dimension of 70 mm in length, 25 mm in width and 0.3 mm in thickness, consistent with ASTM standards. The tensile direction was parallel to the rolling direction. Three tests were conducted on each condition to ascertain reproducibility.

3. Results and discussion

The as-deformed microstructures of the FC and WQ samples are different (see Figure 1) and the details of the microstructures can be found elsewhere [26]. Brief summaries of microstructures are given here: FC samples consist of more equiaxed grains while WQ samples have more elongated grain structure. This can be attributed to the macrostructural differences in the hot rolled stage where the FC sample has equiaxed grains due to RX and grain growth [26]. Grain length, grain width and aspect ratio results are summarized in Table 1. The average lengths are similar in both samples (1000 nm) while the grain width is about one-third smaller in the WQ specimens (230 nm in WQ vs. 350 nm in FC), which corresponds to a higher aspect ratio (4.4 in WQ vs. 2.9 in FC). The larger grain width in the FC sample was caused by grain growth during furnace cooling. Dislocation densities are high in both samples. The average dislocation densities were measured to be $2.3 \times 10^{13}\,m^{-2}$ and $2.2 \times 10^{13}\,m^{-2}$ in the FC and WQ specimens, respectively [26]. Boundary misorientation angle distributions of the FC and WQ specimens are shown in Figure 2. On one hand, the results show that boundary misorientation angles (θ) exhibit a bimodal distribution in the FC sample, in which $\theta < 12°$ and $\theta > 30°$ are dominant. On the other hand, misorientation angles are distributed more evenly from low to high angles in the WQ specimen. High angle boundaries (HABs) are defined as boundaries with misorientation angles greater than 15°, while low angle boundaries (LABs) are boundaries with misorientation angles small than 15° for convenience. Our calculations show that HABs proportions are 39 and 57% for FC and WQ specimens, respectively. The average misorientation angles are computed to be 18° and 25° for FC and WQ specimens, respectively. From the HABs proportion and average misorientation angle data, as well as the grain size, it is demonstrated that the

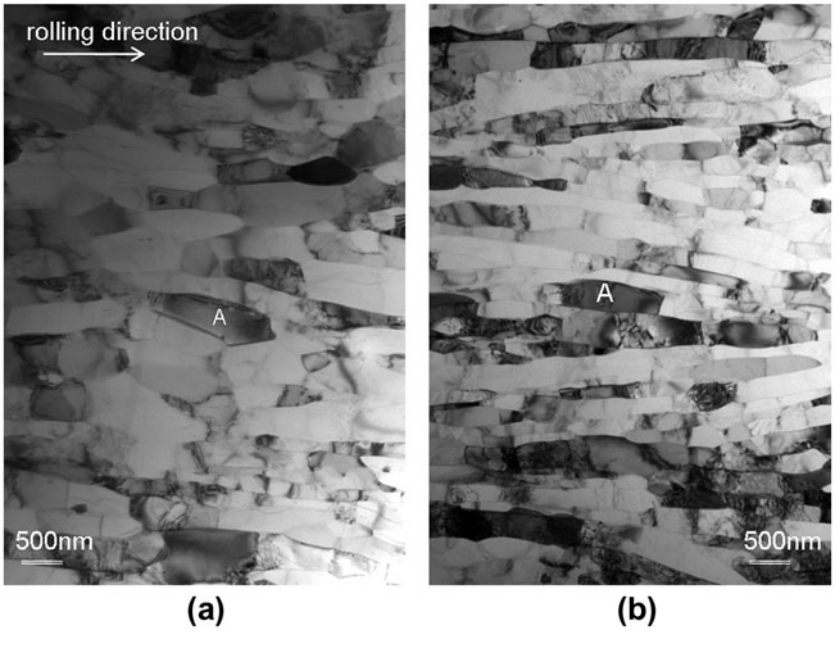

Figure 1. The as-cold rolled microstructures of the (a) FC sample and (b) WQ sample.

Table 1. Microstructure parameters of the as-cold rolled FC and WQ samples.

	Grain length (nm)	Grain width (nm)	Aspect ratio	HABs (%)	ρ (m^{-2})	Average precipitate distance (μm)	Solid solution amount
FC	1000	350	2.9	39	2.3×10^{13}	1	Low
WQ	1000	230	4.4	57	2.2×10^{13}	40	High

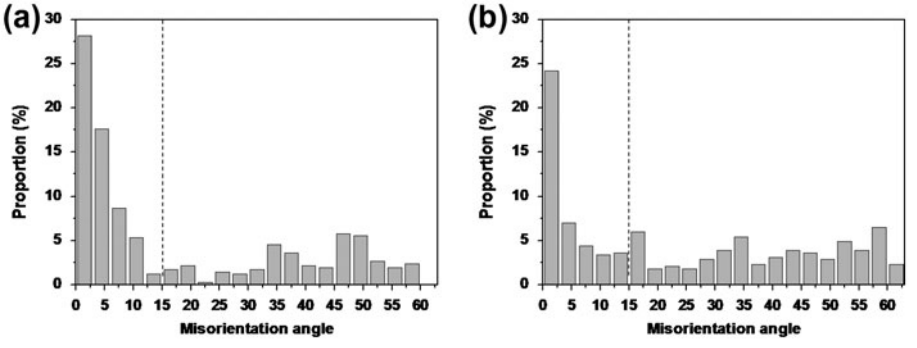

Figure 2. Grain boundary misorientation angle distributions of the (a) FC and (b) WQ specimens.

WQ microstructure primarily consists of UFGs and HABs. In addition to boundary misorientation angle distributions, spatial HAB and LAB arrangements are also summarized in Figure 3. The bold lines indicate HABs, the thin lines represent LABs and the

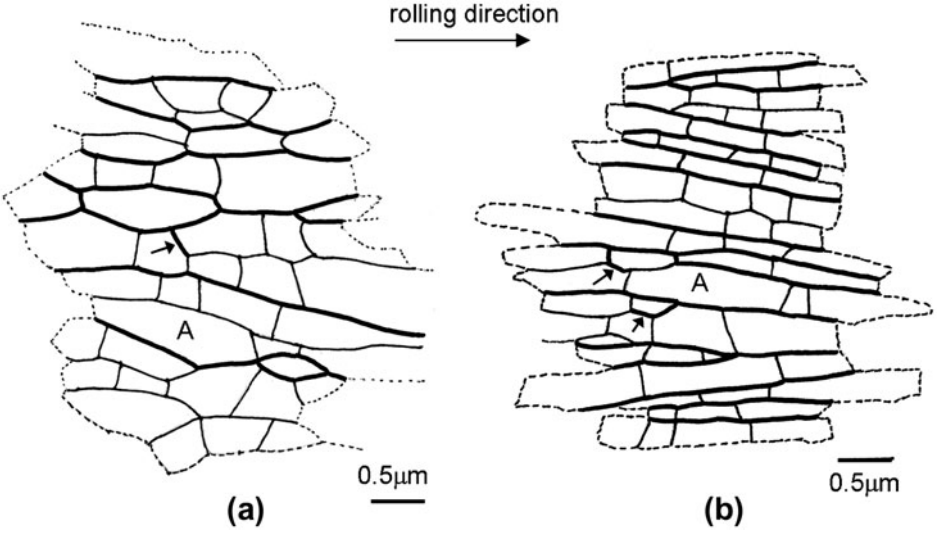

Figure 3. Spatial HAB and LAB distributions of the (a) FC and (b) WQ specimens.

dash lines denote undefined boundary structures. Reference grains are marked with 'A' letters in both Figures 1 and 3 for direct comparison. The spatial boundary distributions reveal that boundaries approximately parallel to the rolling direction are mainly HABs while the transverse boundaries are generally LABs. HAB spacings are observed to be smaller in the WQ specimen than in the FC specimen. As indicated by the arrows in Figure 3, some discontinuous HABs appear in both the FC and WQ samples. It is suggested that metals with intermediate to high stacking fault energies undergo grain subdivision during plastic deformation [29]. HABs can be generated by the occurrence of texture evolution and microstructural evolution [29,30]. The development of discontinuous HABs in the FC and WQ samples is suggested to take place by coalescence of LABs with orientation gradients during microstructural evolution [29,30].

The macrostructures on transverse planes of the FC and WQ specimens annealed at 220–280 °C are shown in Figure 4. Lamellar structures represent the principal feature following cold-rolling in both samples [26]. The lamella spacing is larger in the as-deformed FC sample, relative to that of the WQ sample. When the samples were annealed, the microstructures remain unchanged up to temperatures of 220 °C (Figure 4(a)) and 240 °C (Figure 4(b)) in the FC and WQ samples, respectively, in which the lamellar structures are preserved. RX was evident mostly at the surface of

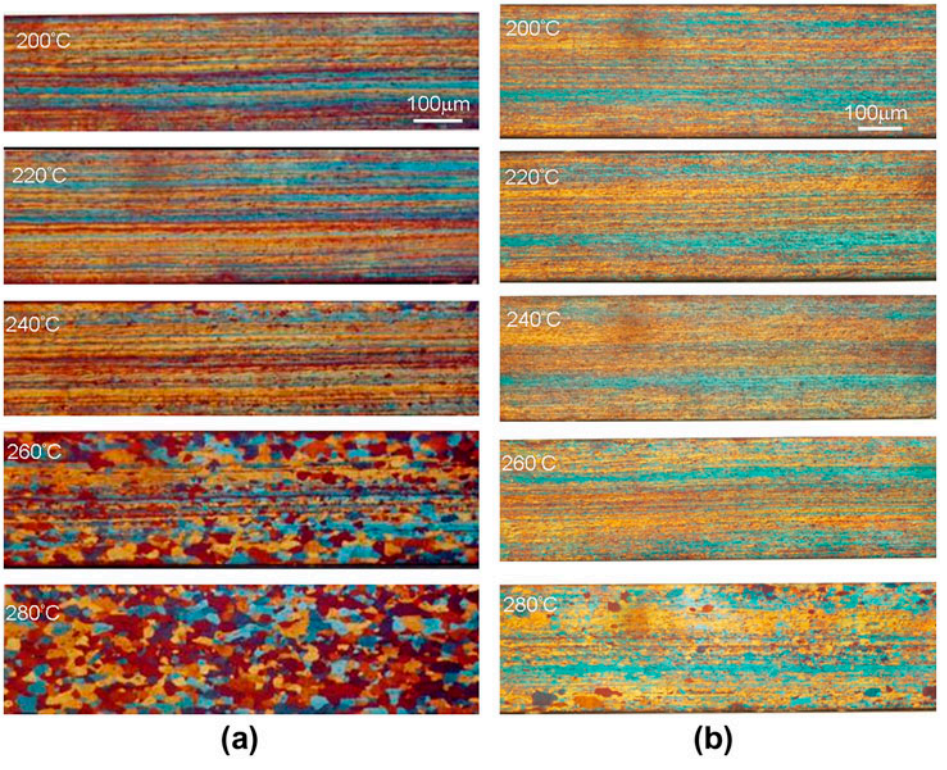

Figure 4. (colour online) Optical micrographs of the (a) FC samples and (b) WQ samples annealed at temperatures ranges from 200 to 280 °C for 1 h.

FC-240 °C annealed specimen (Figure 4(a)), whereas a few recrystallized grains appeared on the WQ-260 °C annealed specimen bottom surface (Figure 4(b)). The RX grain fraction was noted to increase with annealing temperature in both samples. The sample was fully recrystallized at 280 °C in the FC sample (Figure 4(a)), whereas the WQ sample contained a deformed microstructure with a small fraction of RX grains (Figure 4(b)).

The ODFs of the as-cold rolled and some selected annealed FC and WQ samples are shown in Figures 5 and 6, respectively. As expected, the deformation texture after 95% rolling reduction is well described by the α-fibre (Figures 5(a) and 6(a)) and β-fibre (Figures 5(b) and 6(b)) in both conditions, with strong Copper, S and Brass components. The Goss component also exists in the as-rolled FC sample (Figure 5(a)). The as-cold rolled WQ specimen is found to have stronger rolling textures than the as-cold rolled FC specimen. The ODFs of the annealed WQ samples indicates enhanced deformation texture with annealing temperature, in which both Copper and *S* component intensities increase with annealing temperature to 240 °C (Figure 6(b)). After the sample was annealed at 280 °C for 1 h, it consists of both Cube component (Figure 6(c)) and remaining rolling texture (Figure 6(a) and (b)). For the annealed FC samples, rolling texture is slightly enhanced up to annealing temperature of 200 °C (Figure 5(a) and (b)) and Cube component becomes dominant at higher annealing temperatures (Figure 5(c)). As suggested by Jazaer and Humphreys [31], if the heavily deformed materials undergo RX, the deformation texture will be replaced by an annealing texture in which the $\{0\,0\,1\}\langle 1\,0\,0\rangle$ or Cube component is dominant. However, if continuous recrystallization (CRX) occurs, the deformation texture is retained [31]. It is evident that the rolling textures are retained in the annealed WQ samples (Figure 6(b)), which infers the occurrence of CRX in the WQ sample. A discussion on CRX is presented in a subsequent section.

The as-cold rolled WQ specimen was found to have higher YS, UTS and tensile elongation [26] than the as-cold rolled FC specimen, which was attributed to the higher amount of solute atoms existing in the WQ specimen. It is proposed that vacancy concentrations are different in the two cases and affect their mechanical properties. Hot rolling was carried out at a starting temperature of 743 K and a finished temperature of 643 K. Taking the vacancy formation energy of 0.69 eV in aluminium [32], the ratio of vacancies to atoms in the as-hot rolled sample was calculated to be 4×10^{-6}. When the sample is cooled to room temperature, the equilibrium vacancy concentration is substantially reduced to 2.2×10^{-12}. Assume that all the vacancies were retained when the sample was WQ and no excess vacancy was preserved when the sample was slowly cooled (FC). The upper bound of vacancy concentration difference in the hot rolled FC and WQ samples is of the order of 10^6. This order difference of vacancies may be considered to have a significant influence on the mechanical behaviour. Maddin and Cottrell [33] reported that quenched-in vacancies critically influence critical shear stress in a high-purity single crystal Al. However, the critical shear stress difference of the FC and WQ samples gradually diminished with imposing strain. The cause of vacancies in the as-hot rolled WQ sample in the present study cannot be neglected, yet both FC and WQ samples were further cold rolled from a thickness of 6 mm to a final thickness of 0.3 mm equivalent to a total reduction of ~95%. The large amount of imposed strain will initiate multiple dislocation activities (such as dislocation slip, climb and annihilation as well as jog creations, etc.), which involve multiple vacancy generation and

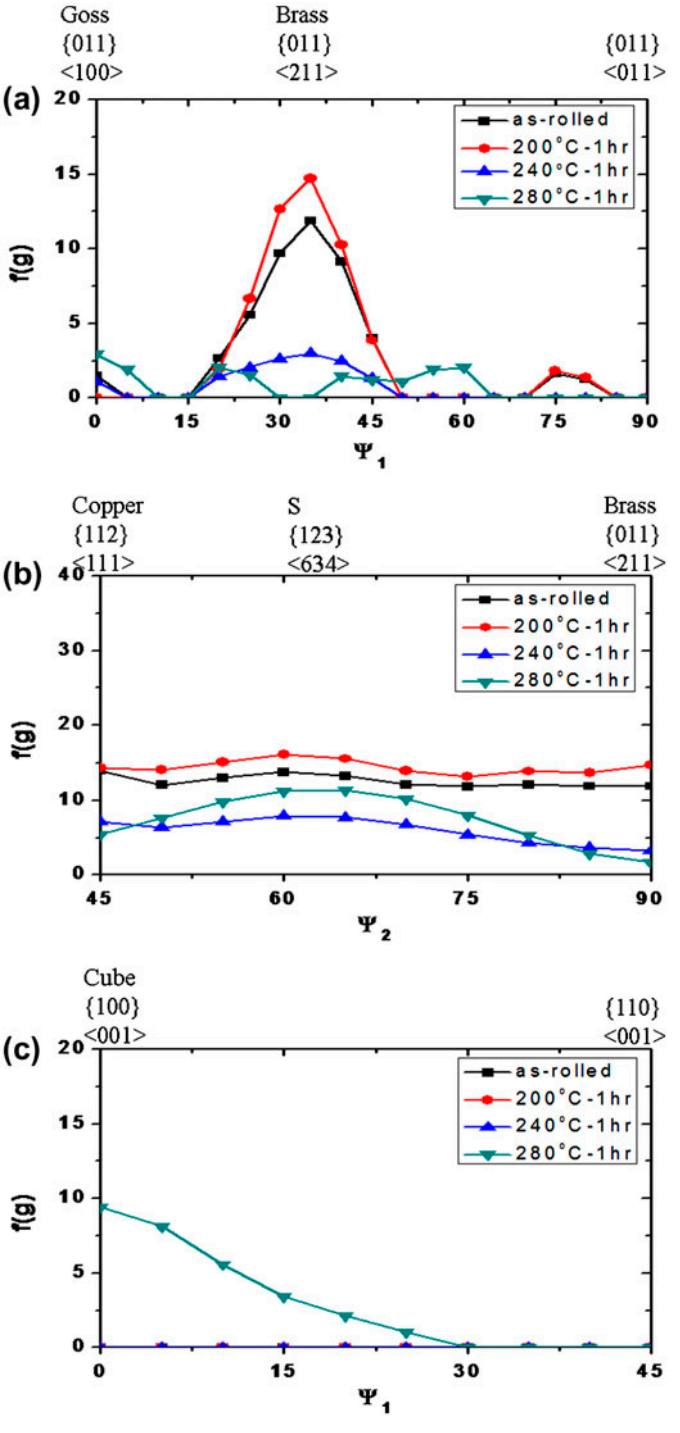

Figure 5. (colour online) ODFs of the as-rolled and selected annealed FC samples (a) α-fibre, (b) β-fibre and (c) cube.

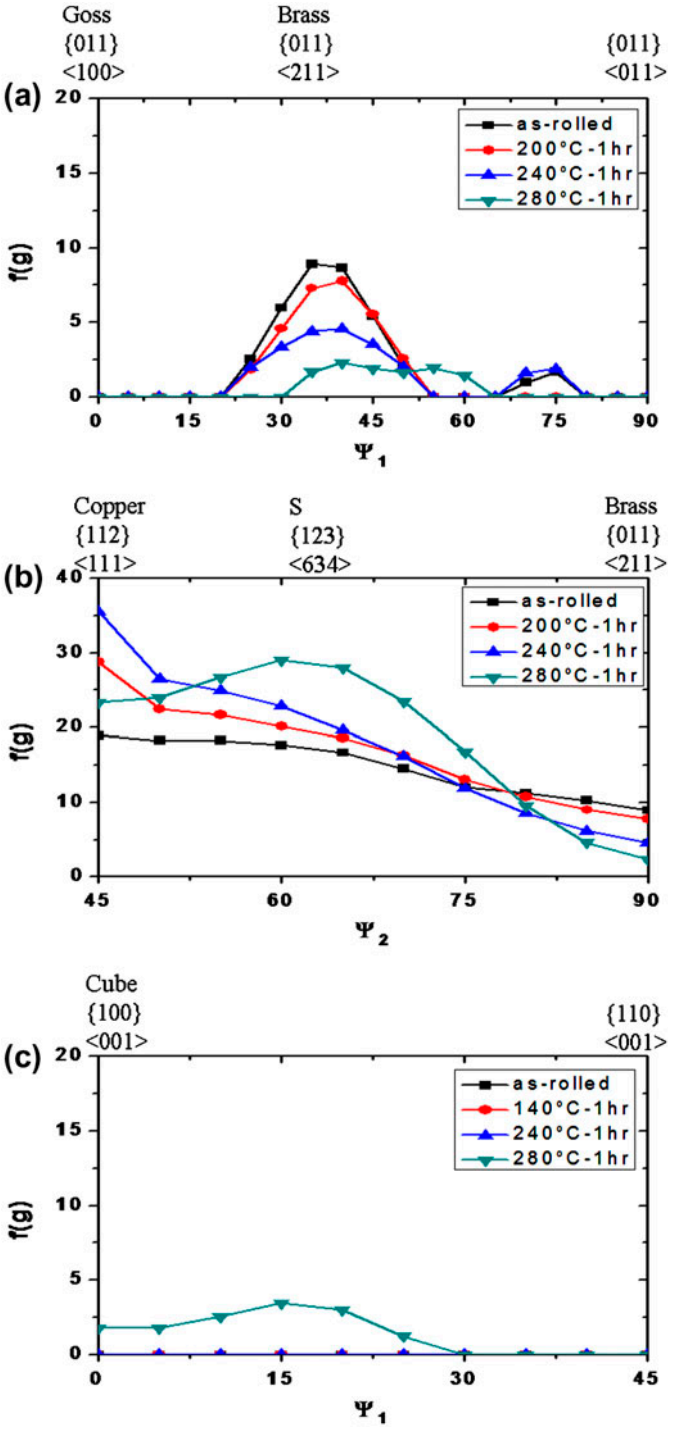

Figure 6. (colour online) ODFs of the as-rolled and selected annealed WQ samples (a) α-fibre, (b) β-fibre and (c) cube.

absorption. Therefore, the effect of vacancy can be excluded on the cold-rolled samples.

It may be suggested that strain rate sensitivities (SRS) of the FC and WQ samples play an important role on the tensile behaviour. May et al. [34] reported that SRS (m) is higher in the commercial purity (AA1050) UFG Al than CG Al. The values were determined to be $m = 0.014$ for the UFG Al and $m = 0.004$ for the CG Al in the strain rate range of 10^{-3} and $10^{-5}\,s^{-1}$ at room temperature. Additionally, a transition of stress–strain curve was observed in their work after strain rate jump (drop) test (a slight increase of stress instead of decrease of stress) and this is related to dynamic strain aging effect. This effect implies that solid solute atoms appear in the aluminium matrix. In related studies, it was also demonstrated that SRS is influenced by the solid solution amount in the aluminium matrix [35,36]. Lee et al. [35] measured the SRS of an Al–Mn alloy (AA3003) homogenized at different temperatures and subsequently deformed by equal channel angular extrusion (ECAE). The SRS of the specimen with a lower amount of Mn in solution was observed to be larger ($m = 0.022$) than the sample with a higher amount of Mn in solution ($m = 0.006$). Kim et al. [36] detailed the pureness of the matrix can affect the recovery rate of pure aluminium and further changes its mechanical behaviour in an Al–Fe–Si alloy (AA8011) subjected to accumulative roll bonding (ARB). The tensile stress–strain curves of this ARBed Al exhibit a steady state, which is resulted of dynamic recovery. Therefore, SRS deformation is taken into account in Considére criterion. It was found that SRS primarily affects the behaviour in the post-uniform or necking region. In the present study, FC sample has more precipitates (purer aluminium matrix), whereas the WQ sample has more solid solution atoms. According to the aforementioned findings [34–36], this can cause a reduction of SRS value in the WQ sample. On one hand, solute atoms in the matrix can decrease SRS in Al alloys. Therefore, SRS in the WQ sample is reduced. On the other hand, the grain size of the WQ sample was measured to be smaller than that corresponding to the FC sample, which in turn can raise its SRS value [34,37]. Hence on the basis of the combined, and opposing, effects of grain size and solid solution, it is suggested that SRS values are comparable for the two conditions (FC vs. WQ) and thus have limited influence on tensile behaviour.

The variations in tensile YS as a function of annealing temperatures of the annealed FC and WQ specimens are shown in Figure 7(a). The reported YS values were averaged from three individual tests. Error bars of all tests are plotted along with the curve to show the deviations of three tests for each condition and it shows good reproducibility. The YS decreases with annealing temperature in both samples. However, the decrease is less obvious below 240 and 260 °C for the FC- and WQ-specimen, respectively. The YS of the FC sample changes from 162 ± 1.9 MPa at the as-deformed state to 110 ± 0.7 MPa (equivalent to 0.68YS of the as-cold rolled sample) when it was annealed at 240 °C for 1 h. The drop in YS for the WQ specimen is from 178 ± 1.2 MPa of the as-deformed specimen to 123 ± 0.9 MPa (equivalent to 0.69YS of the as-cold rolled sample) of the specimen annealed 260 °C for 1 h. The slopes of both curves are similar for both samples. After the samples were annealed at high temperature for 1 h, both materials were fully annealed. The isothermal annealing response of the two materials at 240 °C is shown in Figure 7(b). The two curves show dramatically different behaviour. The decrease of YS in WQ samples is slow and with a constant rate as the annealing time increases from 10 to 480 min, while the YS in FC samples decreases

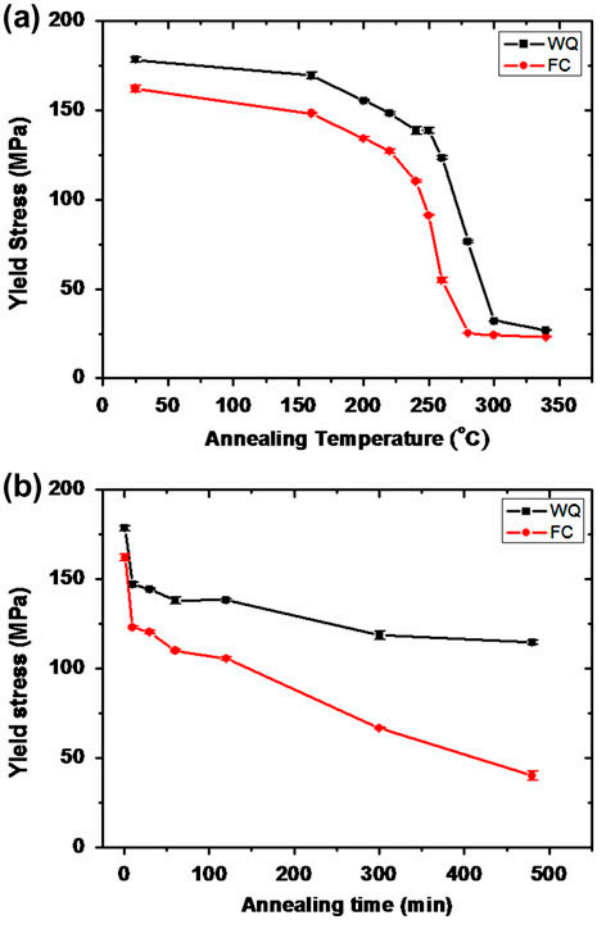

Figure 7. (colour online) YS variations of the (a) isochronal annealed and (b) isothermal annealed FC and WQ samples.

very rapidly even for 120 min. The WQ sample annealed at 240 °C for 480 min still shows YS of 114.5 ± 1.2 MPa, which equivalent to 0.64 of the as-cold rolled YS. On the other hand, the FC sample only possesses 40 ± 2.4 MPa (equivalent to 0.25YS of the as-cold rolled sample) when the sample was annealed at 240 °C for 480 min.

Examination of the transverse planes of the annealed WQ samples shows that no RX grains are formed even at the annealing time of 480 min while as RX grains appeared after 60 min annealing time in the FC samples (Figure 8). The decrease in YS in the isothermally annealed WQ samples was mainly caused by dislocation recovery. It is clear that the WQ specimen has better thermal stability than the FC specimen. In the literature, the same material (AA1050) subjected to ECAE to a von Mises strain of ~8 exhibited a continuous grain coarsening process during annealing at annealing temperatures below 275 °C [38]. This is attributed to the stable microstructure in the as-ECAEed state, in which equiaxed submicrometer grains with high fraction of HABs

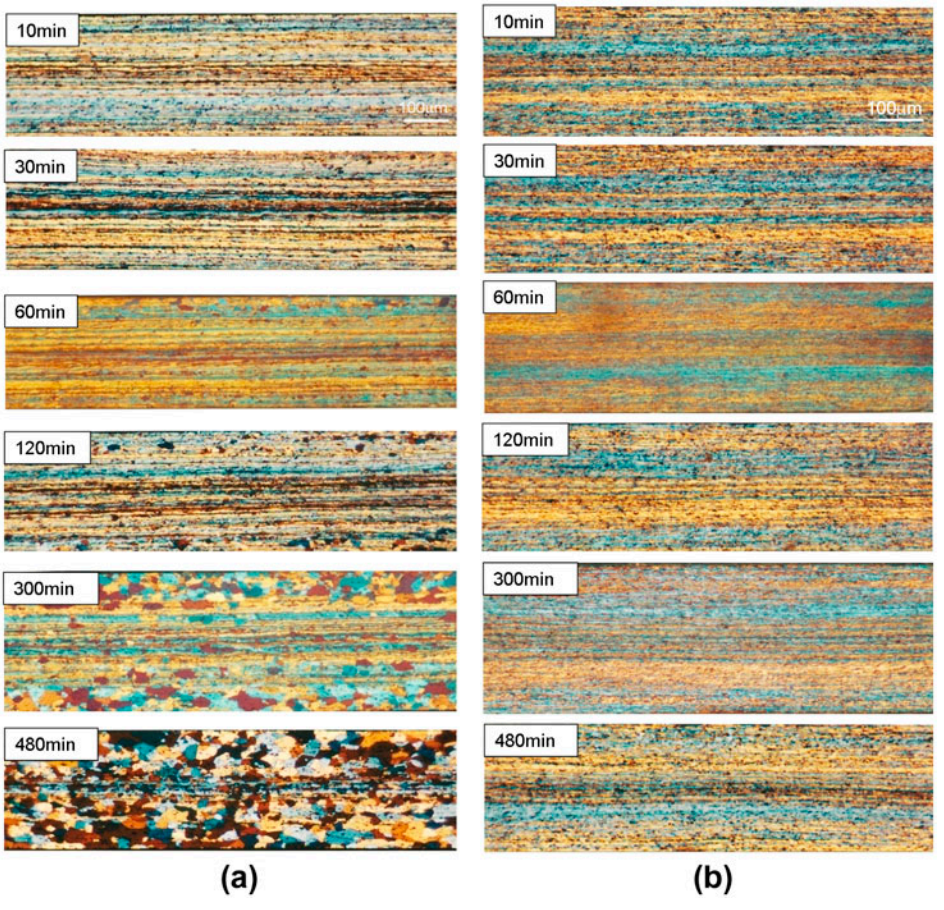

Figure 8. (colour online) Optical micrographs of the (a) FC and (b) WQ samples annealed at 240 °C for different time periods.

are the main feature. Oscarsson et al. [39] showed that when the rolling reduction is greater than 95% in a strip cast aluminium, CRX occurs when the material is annealed. CRX implies that grain structures are geometrically similar at all stages, only changing in scale as annealing progresses. At the high reduction levels (>95%), the boundaries are mostly HABs and the microstructure tends to coarsen in a gradual way with increasing temperature. In this work, the WQ specimen has an UFG structure with high proportion of HABs. Hence, CRX is expected to happen when the sample is annealed at lower temperatures. The enhanced rolling texture on the annealed WQ samples supports this phenomenon (Figure 6). It is therefore concluded that the presence of a small amount of solid solute atoms in the WQ specimen can not only refine grain size further but also promote high fraction of HABs. This microstructure undergoes grain coarsening or CRX during annealing treatment and RX can be delayed to a higher temperature.

As mentioned in the earlier section, the strategy of using bi-modal or multi-modal materials to obtain a balance in strength and ductility has been investigated for

numerous material systems. However, in most cases, the ductility of bi-modal or multi-modal materials decreases as the strength is increased, and vice versa. In related work, Zhao et al. [21,27] used simple rule to categorize bimodal materials into one of three possible cases: positive (improved), negative (diminished) and rule-of-mixtures. A positive deviation means that data points are above the line predicted by the rule of mixtures whereas a negative deviation means that the data points fall below rule of mixtures line. An example of positive deviation was reported by Wang et al. [2]; an introduction of 25% volume fraction of CGs into an UFG Cu matrix resulted in a 30% uniform elongation and a comparable elongation to failure (65%) with that of the CG Cu counterpart (70%), while the yield strength can still be maintained about 5–6 times higher than that of the CG Cu. Similar results were reported by Jin et al. [40] with a 5754 Al-3.1 Mg-0.3 Mn-0.2 Fe-0.1 Si alloy (wt.%). In contrast, a negative deviation from the rule-of-mixtures was observed during thermal annealing of nanocrystalline Cu prepared by dynamic plastic deformation at liquid nitrogen temperature [41]. However, many experimental and modelling studies also show that a materials strength and ductility follow a rule-of-mixtures prediction when the nanograins (NG) and CG were distributed homogeneously [21,27,42,43]. The annealed samples used in present study contain a bimodal grain structure; in which RX grains spatially distributed at the specimen surface while deformed UFG remains within the specimen centre. The tensile engineering stress and strain are plotted in Figure 9. As shown in Figure 9, tensile stress decreases while ductility remains unchanged at low annealing temperatures in both the annealed FC and WQ samples. When annealing temperature is larger than about 200 °C, tensile stress decreases and elongation increases with increasing annealing temperature. The plots of YS vs. total elongation and UTS vs. uniform elongation of the annealed FC and WQ samples are shown in Figure 10(a) and (b). The results reveal that the YS decreases sharply at low annealing temperatures, and then linearly approaches the values corresponding to fully coarse-grained samples. As the YS is plotted as a function of RX grain fraction (Figure 10(c)), it shows the YS decreases rapidly at the beginning of RX, and then linearly trends to the value of the coarse-grained sample, resulting in a slight negative deviation from the of rule-of-mixtures prediction. However, when

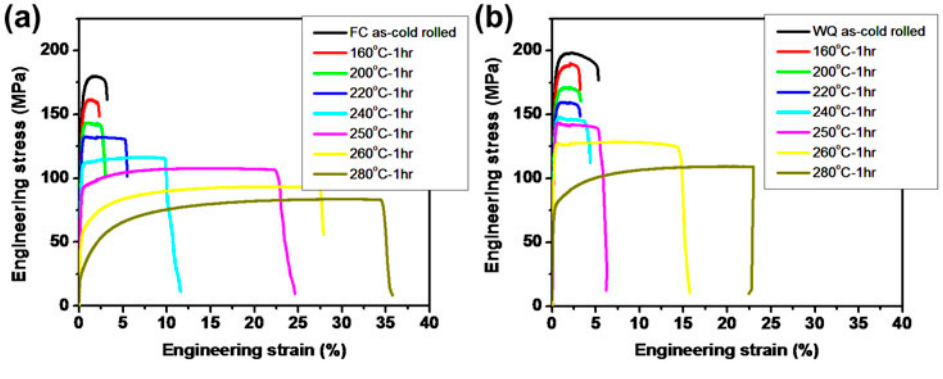

Figure 9. (colour online) Tensile engineering stress–strain curves of the as-deformed and annealed FC and WQ samples.

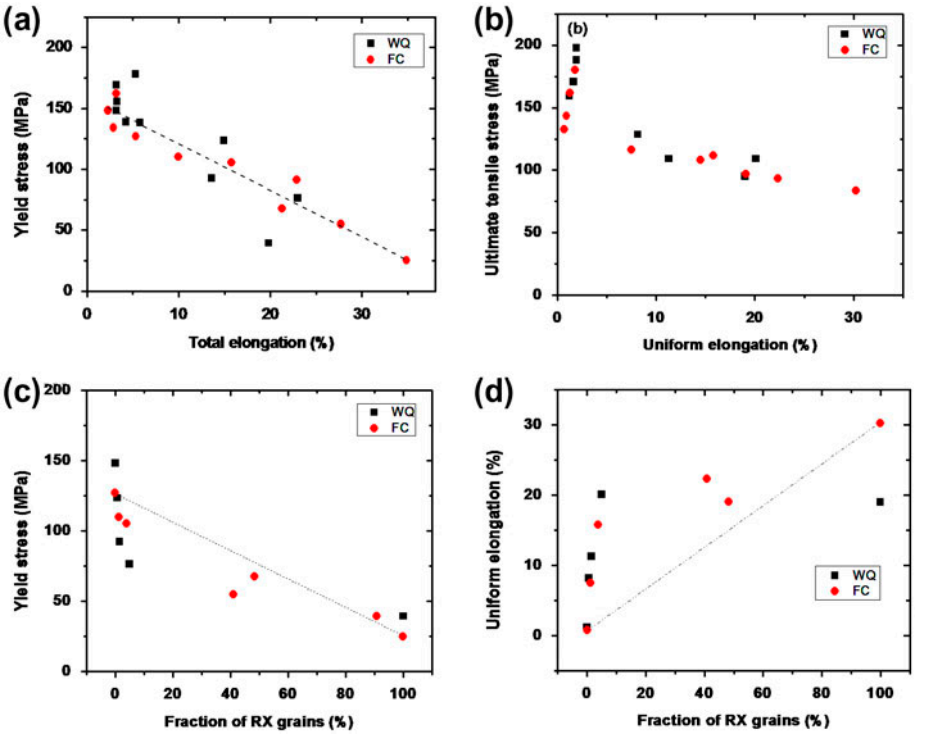

Figure 10. (colour online) (a) YS vs. total elongation, (b) UTS verses uniform elongation, (c) YS verses the RX volume fraction and (d) uniform elongation vs. the RX volume fraction of the bi-modal aluminium.

uniform elongation is plotted as a function of RX grain fraction (Figure 10(d)), it shows that uniform elongation increases rapidly and then stabilizes at a value corresponding to that of the recrystallized sample, resulting in a slight positive deviation from the rule-of-mixtures prediction. According to Zhao et al. [21,27], these differences in the relationship between uniform elongation and RX grain fraction may be attributed to differences in microstructural characteristics, such as different spatial distributions of the UFG and CG grains, and/or possibly to different size differences between the scales of the micro-grains and the UFG matrix. It can be noticed that RX grains appear on the sample surfaces and the centre area remains the cold rolled structure in the annealed FC and WQ samples (Figures 4 and 8). Clearly, this arrangement is far from a random distribution of micro-grain agglomerates heterogeneously distributed throughout the UFG/NC matrix. Recently, Fang et al. [44] fabricated a microstructure with NG on the sample surface and CG at the centre. Tensile tests revealed that this microstructure has YS twice of that in CG sample and the ductility can remain comparable to the CG sample. The distribution of NG and CG is reverse to the present work, while both result in the deviation from the rule-of-mixtures prediction [44]. Considering the homogeneous distribution of NG and CG caused a rule-of-mixture prediction [21,27], therefore, it is suggested that this spatial distribution of RX grains in the current work may be

responsible for the observed deviation from the rule-of-mixtures prediction. Moreover, the dislocation recovery and grain coarsening at the beginning of annealing treatment might be another reason for the deviations from the rule-of-mixtures: a decrease of dislocation density could cause a rapid decrease in stress and an increase in ductility [45].

4. Conclusions

In summary, two conclusions can be drawn from this work. First, it is shown that with higher content of solid solution atoms in the WQ aluminium the RX temperature can be postponed to a higher temperature. Second, the relationship between YS and RX grain fraction (Figure 10(c)) as well as the relationship between uniform elongation and RX grain fraction (Figure 10(d)) reveal slight deviations from the rule of mixtures prediction. This may be attributed to the different spatial distributions of the UFG and CG grains.

Acknowledgements

This work was supported by the National Science Council of ROC under contract NSC-97-2221-E-035-012 and NSC-98-2221-E-035-015. Y.H. Zhao would like to thank the support from National Natural Science Foundation of China (Nos. 51225102 and 2012CB932203) and the Fundamental Research Funds for the Central Universities (No. NUST2012ZDJH008). E.J. Lavernia Gratitude is also extended to *Mr Rodney Peterson* and *Dr William Golumbfskie* of the *Office of Naval Research* for funding to support this work (ONR Contract N00014-12-C-0241).

References

[1] K. Zhang, J.R. Weertman and J.A. Eastman, Appl. Phys. Lett. 87 (2005) p.061921.
[2] Y. Wang, M.W. Chen, F.H. Zhou and E. Ma, Nature 419 (2002) p.912.
[3] P.L. Sun, C.Y. Yu, P.W. Kao and C.P. Chang, Scr. Mater. 52 (2005) p.265.
[4] R. Birringer, Mater. Sci. Eng. A 117 (1989) p.33.
[5] A. Kumpmann, B. Günther and H.-D. Kunze, Mater. Sci. Eng. A168 (1993) p.165.
[6] C.H. Moelle and H.J. Fecht, NanoStruct. Mater. 6 (1995) p.421.
[7] L. Lu, N.R. Tao, L.B. Wang, B.Z. Ding and K. Lu, J. Appl. Phys. 89 (2001) p.6408.
[8] H. Natter, M. Schmelzer and R. Hempelmann, J. Mater. Res. 13 (1998) p.1186.
[9] C.C. Koch, R.O. Scattergood, K.A. Darling and J.E. Semones, J. Mater. Sci. 43 (2008) p.7264.
[10] K. Boylan, D. Osstrander, U. Erb, G. Palumbo and K.T. Aust, Scr. Metall. Mater. 25 (1991) p.2711.
[11] A. Michels, C.E. Krill, H. Ehrhardt, R. Birringer and D.T. Wu, Acta Mater. 47 (1999) p.2143.
[12] Z. Gao and B. Fultz, NanoStruct. Mater. 4 (1994) p.939.
[13] A.J. Detor and C.A. Schuh, Acta Mater. 55 (2007) p.371.
[14] K.A. Darling, B.K. VanLeeuwen, C.C. Koch and R.O. Scattergood, Mater. Sci. Eng. A 527 (2010) p.3572.
[15] T. Frolov, K.A. Darling, L.J. Kecskes and Y. Mishin, Acta Mater. 60 (2012) p.2158.
[16] T. Chookajorn, H.A. Murdoch and C.A. Schuh, Science 337 (2012) p.951.

[17] Y.H. Zhao, Y.T. Zhu and E.J. Lavernia, Adv. Eng. Mater. 12 (2010) p.769.
[18] M. Legros, B.R. Elliott, M.N. Rittner, J.R. Weertman and K.J. Hemker, Philos. Mag. A 80 (2000) p.1017.
[19] V.L. Tellkamp, A. Melmed and E.J. Lavernia, Metall. Mater. Trans. A 32 (2001) p.2335.
[20] Y.H. Zhao, T. Topping, J.F. Bingert, J.J. Thornton, A.M. Dangelewicz, Y. Li, W. Liu, Y.T. Zhu, Y.Z. Zhou and E.J. Lavernia, Adv. Mater. 20 (2008) p.3028.
[21] Y.H. Zhao and E.J. Lavernia, *Mechanical properties of multi-scale metallic materials*, in *Nanostructured Metals and Alloys: Processing, Microstructure, Machanical Properties and Applications*, S.H. Whang, ed., Woodhead Publishing, Cambridge, March 2011, p.375.
[22] P.L. Sun, E.K. Cerreta, J.F. Bingert, G.T. Gray III and M.F. Hundley, Mater. Sci. Eng. A464 (2007) p.343.
[23] Y.H. Zhao, Y.T. Zhu, X.Z. Liao, Z. Horita and TG. Langdon, Appl. Phys. Lett. 89 (2006) p.121906.
[24] P.L. Sun, Y.H. Zhao, J.C. Cooley, M.E. Kassner, Z. Horita, T.G. Langdon, E.J. Lavernia and Y.T. Zhu, Mater. Sci. Eng. A 525 (2009) p.83.
[25] Y.H. Zhao, X.Z. Liao, S. Cheng, E. Ma and Y.T. Zhu, Adv. Mater. 18 (2006) p.2280.
[26] P.L. Sun, Y.H. Zhao, T.Y. Tseng, J.R. Su and E.J. Lavernia, Mater. Sci. Eng. A 527 (2010) p.5287.
[27] Y.H. Zhao, T. Topping, Y. Li and E.J. Lavernia, Adv. Eng. Mater. 13 (2011) p.865.
[28] V. Randle, *The measurement of Grain Boundary Geometry*, Institute of Physics, Bristol, 1993.
[29] D.A. Hughes and N. Hansen, Acta Mater. 45 (1997) p.3871.
[30] P.L. Sun, P.W. Kao and C.P. Chang, Scr. Mater. 51 (2004) p.565.
[31] H. Jazaeri and F.J. Humphreys, Acta Mater. 52 (2004) p.3251.
[32] R. Abbaschian, L. Abbaschian and R.E. Read-Hill, *Physical Metallurgy Principles*, Cengage Learning, Stamford, CT, 2010.
[33] R. Maddin and A.H. Cottrell, Philos. Mag. 46 (1955) p.735.
[34] J. May, H.W. Höppel and M. Göken, Scr. Mater. 53 (2005) p.189.
[35] I.S. Lee, Y.S. Lee, P.W. Kao and C.P. Chang, *Nanometals – status and perspective*, in *Proceedings of 33rd Risø International Symposium on Materials Science*, S. Fæster, N. Hansen, X. Huang, D.J. Jensen and B. Ralph, eds., Riso National Laboratory and Riso, Roskilde, 2012, p.295
[36] H.W. Kim, S.B. Kang, N. Tsuji and Y. Minamino, Acta Mater. 53 (2005) p.1737.
[37] H. Miyamoto, K. Ota and T. Mimaki, Scr. Mater. 54 (2006) p.1721.
[38] C.Y. Yu, P.L. Sun, P.W. Kao and C.P. Chang, Mater. Sci. Eng. A 366 (2004) p.310.
[39] A. Oscarsson, H.-E. Ekström and B. Hutchinson, Mater. Sci. Forum 113–115 (1993) p.177.
[40] H. Jin and D.J. Lloyd, Scr. Mater. 50 (2004) p.1319.
[41] Y.S. Li, Y. Zhang, N.R. Tao and K. Lu, Scr. Mater. 89 (2008) p.475.
[42] B. Raeisinia, C.W. Sinclair, W.J. Poole and C.N. Tome, Modell. Simul. Mater. Sci. Eng. 16 (2008) p.025001.
[43] S.P. Joshi, K.T. Ramesh, B.Q. Han and E.J. Lavernia, Metall. Mater. Trans. A 37 (2006) p.2397.
[44] T.H. Fang, W.L. Li, N.R. Tao and K. Lu, Science 331 (2011) p.1587.
[45] Y.H. Zhao, J.F. Bingert, Y.T. Zhu, X.Z. Liao, R.Z. Valiev, Z. Horita, T.G. Langdon, Y.Z. Zhou and E.J. Lavernia, Appl. Phys. Lett. 92 (2008) p.081903.